ACS APPLIED MATERIALS & INTERFACES

Research Article

www.acsami.org

Ceragenin Mediated Selectivity of Antimicrobial Silver Nanoparticles

Mark A. Hoppens,[†] Christopher B. Sylvester,[†] Ammar T. Qureshi,[†,⊥] Thomas Scherr,[‡,⊥] Desiree R. Czapski,[§] Randolph S. Duran,[§] Paul B. Savage,[∥] and Daniel Hayes*[,†]

[†]Department of Biological and Agricultural Engineering, Louisiana State University and LSU Agcenter, 149 E. B. Doran Building, Baton Rouge, Louisiana 70803, United States

[‡]Cain Department of Chemical Engineering, Louisiana State University, Baton Rouge, Louisiana 70803, United States

[§]Department of Chemistry, Louisiana State University, 603 Choppin Hall, Baton Rouge, Louisiana 70803, United States

[∥]Department of Chemistry and Biochemistry, Brigham Young University, Provo, Utah 84602, United States

Supporting Information

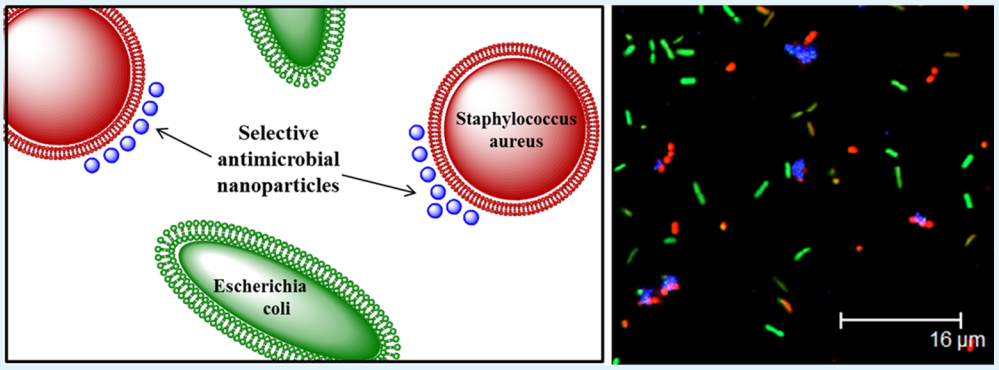

ABSTRACT: The understanding that common broad-spectrum antimicrobials disrupt natural microbial flora important in acquiring nutrients and preventing infection has resulted in a paradigm shift favoring more selective antimicrobials. This work explores silver nanoparticles conjugated with ceragenin, or cationic antimicrobials (CSA-SNPs), as a potential Gram-positive selective antimicrobial. Herein, CSA-SNPs are characterized using transmission electron microscopy (TEM), dynamic light scattering (DLS), zeta potential, and high-performance liquid chromatography−electrospray time-of-flight mass spectrometry (HPLC−ESI-TOF-MS). The antimicrobial properties are determined through minimum inhibitory concentration/minimum bactericidal concentration (MIC/MBC) and time-kill studies. Spatial selectivity of the conjugate nanoparticle was evaluated using confocal imaging, MATLAB statistical analysis, and video monitored interactions between bacteria and CSA-SNPs via laser trapping techniques. Cytotoxicity was also determined by live/dead staining and flow cytometry. Average particle size, as determined through TEM analysis, and hydrodynamic diameter, as determined via DLS, are 63.5 ± 38.8 and 102.23 ± 2.3 nm, respectively. The zeta potential of the SNP before and after CSA attachment is −18.23 and −8.34 mV, respectively. MIC/MBC data suggest that CSA-SNPs are 8 times more effective against *Staphylococcus aureus* than SNPs alone. Furthermore, MATLAB analysis of confocal imaging found that 70% of CSA-SNPs are within 2 μm of *S. aureus*, whereas this percentage falls to below 40% with respect to *Escherichia coli*. These results are bolstered further by laser trapping experiments demonstrating selective adherence of CSA-SNPs conjugates with bacterial strains. Cytotoxicity studies of CSA-SNPs against 3T3 fibroblasts indicate 50% cell viability at 50 ppm.

KEYWORDS: *selective antimicrobial, conjugate nanoparticle, specific binding, ceragenin*

1. INTRODUCTION

A significant source of difficulty in treating infections is the broad-spectrum activity of state-of-the-art antibiotics. In an attempt to eliminate pathogenic microbes, many antibiotic treatments also kill or inhibit natural microbial flora.[1] Indigenous microbiota aid in acquiring nutrients and provide protection against colonization by pathogenic microorganisms.[1] When these natural bacterial populations become compromised, opportunistic pathogens such as *Clostridium difficile*, *Candida ablicans*, and *Staphylococcus aureus* can impair post-treatment recovery or require additional treatment.[1−4] Selective antimicrobial agents aim to treat infections while leaving the native microbiome unaffected.

Advances in the chemistry of inorganic nanoparticles have led to a rapid increase in the number of types and potential uses for nanoparticles.[5−8] Nanoparticles can be facilely manufactured from a large variety of materials and in a variety of shapes, sizes, number of layers, and surface chemistries. An area of

Received: May 26, 2014
Accepted: July 23, 2014
Published: July 23, 2014

particular interest is the use of nanoparticles as a vehicle for the delivery of drugs.[7] Nanoparticles offer a high surface area-to-volume ratio, allowing high drug carrying capacity, and can be targeted to infected tissues and regions to deliver sustained drug treatment.[9−11] Ligands attached to nanoparticles are also less prone to degradation than those free in solution.[11] Additionally, amphiphilic molecules with thiol groups self-assemble on noble metals such as silver or gold.[12,13] It has also been demonstrated that particles less than 200 nm in diameter are more likely than larger nanoparticles to remain in circulation in vivo.[11] The composition, morphology, and surface chemistry of nanoparticles can be manipulated, making them excellent candidates for selective antimicrobials.

Silver has long been known to have antimicrobial properties, and correspondingly, silver nanoparticles (SNPs) and other silver nanomaterial compositions have been shown to possess similar antimicrobial properties.[5,14−18] Silver is currently used as an antimicrobial in several products including bandages, antibacterial gels, and catheters.[19] Silver impacts microbial systems through several mechanisms, resulting in the disruption of many crucial cell functions such as cell wall and nucleic acid synthesis, translation, protein structure, and membrane ion pumps. Without these functions, cell division inhibition or death often occurs. This combination of potent antimicrobial activity and limited cytotoxicity makes SNPs potentially favorable as an alternative to traditional antibiotics as a treatment for infections.

Natural cationic peptides display potent antimicrobial properties with low rates of resistance and varying levels of selectivity. However, many are vulnerable to protease activity, limiting their usefulness as an antibiotic in vivo.[20,21] Ceragenins, also called CSAs, are synthetic molecules designed to mimic the activities of these naturally occurring antimicrobial peptides.[22] CSAs have been demonstrated as effective antimicrobials against drug-resistant strains of *Pseudomonas aeruginosa*,[23] *Helicobacter pylori*,[24] *S. aureus*,[25] and periodontic bacteria such as *Streptococcus mutans* and *Porphyromonas* species.[26] A novel ceragenin used in this study, CSA-124, has been synthesized with a terminal thiol group, allowing for specific covalent bonding to noble metals.

Herein, we describe the synthesis of a CSA-124 conjugated SNP (CSA-SNP) with improved antimicrobial activity and physical selectivity for *S. aureus*. The particles composition and physical properties are explored through transmission electron microscopy (TEM), dynamic light scattering (DLS), inductively coupled plasma-optical emission spectrometry (ICP-OES), and liquid chromatography−electrospray ionization tandem mass spectrometry (LC−ESI-MS). The antimicrobial efficacy is demonstrated with standard minimum inhibitory concentration/minimum bactericidal concentration (MIC/MBC) and time-kill assays. Mammalian cytotoxicity of the CSA-SNP constructs are quantified using live/dead staining and flow cytometry, and hemolytic characterization is assessed via an ASTM standard. Physical selectivity is demonstrated both qualitatively and quantitatively through confocal microscopy and laser trapping analysis.

2. MATERIALS AND METHODS

2.1. Materials. SmartSilverAS was purchased from NanoHorizons, Inc. (Bellefonte, PA). Dialysis membranes (10 000 Da) were ordered from Sigma-Aldrich. TEM grids and paraformaldehyde (16%) were obtained from Electron Microscopy Sciences (Hatfield, PA). The Acclaim Mixed-Mode HILIC-1 normal phase LC column was ordered from ThermoScientific (Logan, UT). For cell culture, DMEM-RS, trypsin (0.25%, 1× solution), and DPBS/modified (1×) are HyClone products and are also ordered through ThermoScientific. Sytox Red dead cell stain was purchased from Molecular Probes by Life Technologies Corporation, and a Live BacLight Bacterial Gram Stain Kit was purchased from Invitrogen Molecular Probes (Eugene, OR). CSA-124 was prepared at Brigham Young University by functionalizing an early lead ceragenin, CSA-13, with a thiol group on a short PEG tether. Synthetic details for CSA-124 will be reported elsewhere. All other chemicals were used as received unless otherwise noted. For bacterial culture, Mueller Hinton Broth (MHB) and nutrient agar, pH 6.0 with 0.8% NaCl, were purchased from Himedia/VWR, and Mannitol Salt Agar was purchased from Acumedia/Neogen Corporation (Lansing, MI).

2.2. Methods. *2.2.1. Conjugating Silver Nanoparticles with CSA-124.* A 4 mL suspension of SNPs in deionized (DI) water at 300 ppm was mixed with 50 μL of CSA-124 in DI water at 0.2 mM. This solution was allowed to react overnight at room temperature and was then purified in dialysis sacks, pore size 12 000 Da MWCO, for 24 h. During this time, the water was changed three times.

2.2.2. Dynamic Light Scattering (DLS). Hydrodynamic diameters were measured using a Malvern Zetasizer Nano series instrument (Worcestershire, U.K.). NP samples from various stages of synthesis were diluted to roughly 0.02 ppm in $NaHCO_3$/DI (100 mM) then filtered using a Thermo Scientific Nalgene 0.2 μm surfactant-free cellulose acetate membrane. Samples were measured in Malvern ZEN0040 disposable cuvettes at 25 °C. In our determination of zeta potential, NPs were suspended in DI; the solution was then placed in a Zetasizer Nano series folded capillary cell, and zeta potential was measured using a Malvern Zetasizer Nano series instrument (Worcestershire, U.K.) at 25 °C.

2.2.3. Transmission Electron Microscopy (TEM). The TEM images were obtained using a JEOL 2011 (Tokyo, Japan). Nanoparticle samples were diluted to roughly 25 ppm in DI water and 5 μL was applied to an Electron Microscopy Sciences carbon film 400 square mesh copper grid and allowed to air-dry. Images were taken at 150 000×. TEM images were analyzed using Metamorph Advanced software. The diameters of 25 nanoparticles of each type were measured using digital calipers, and statistical significance was determined using a one sample *t* test.

2.2.4. CSA Quantification. A five point standard curve, $R^2 = 0.9942$, was constructed by comparing known concentrations of CSA-124 dissolved in 25% (v/v) acetonitrile (ACN) in DI water to the integrated area of its HPLC−ESI-TOF-MS peak. CSA-124 was displaced from the SNP and run through HPLC−ESI-MS/MS, then quantified by comparison to this standard curve. To remove CSA from the SNP, we added 5.5 μL of DL-dithiothreitol (DTT) to 500 μL of CSA-SNPs and allowed the mixture to react for 1 h at 37 °C. The DTT displaced the CSA from the SNP surface, resulting in DTT-SNPs and a solution of CSA and unreacted DTT. Particles were then separated via centrifugation for 15 min at 12*g*. The supernatant was removed and concentrated from 500 to 250 μL by vacufugation, and 250 μL of ACN/DI (50% v/v) was then added to the solution, bringing the final solution to 25% ACN, mirroring the standard curve solution. The samples were then analyzed by HPLC−ESI-TOF-MS (Agilent 1200 with a binary pump/Agilent ESI TOF 6210, Palo Alto, CA). The LC column used was a normal phase Acclaim Mixed-Mode HILIC-1, 3 μm Analytical (2.1 × 150 mm). Samples and standards were injected at 2 μL. The first mobile phase was 90% ACN in water with 0.1% formic acid, while the second mobile phase was water with 0.1% formic acid. The ESI parameters used are as follows: nitrogen temperature, 325 °C; nitrogen flow, 5 L/min; and nebulizer pressure, 20 psi. The DTT-SNP pellet obtained from the previously mentioned centrifugation was quantified by ICP-OES.

2.2.5. Cytotoxicity Analysis. Murine 3T3 fibroblast cells were seeded onto 12 well plates in 500 μL of growth medium (DMEM, 10% FBS) and allowed to grow for 48 h until 80% confluent. The medium was then replaced with 600 μL of medium containing incremental concentrations of CSA-SNPs. Live controls received 600 μL of the growth medium containing no CSA-SNPs. Dead controls received

600 μL of growth medium and 150 μL of 70% ethanol solution. The cells were incubated at 37 °C in 5% CO_2.

The 3T3 cells were incubated in the CSA-SNP medium for 24 h. Then the medium was removed and collected. The cells were lifted from the 12 well plates using Trypsin and collected in combination with the previously removed media. The cells were then separated through centrifugation and resuspended in 1 mL of phosphate-buffer saline (PBS; −Ca, −Mg). The cells were stained for viability using Sytox Red, 1 μL for 15 min, then separated via centrifugation and fixed in 350 μL of 1% polyformaldehyde (PFA) solution. The live and dead counts were evaluated using flow cytometry.

2.2.6. Hemolytic Characterization. The hemolytic properties of CSA-SNP were assessed using the ASTM E2524-08 Standard Test Method for Analysis of Hemolytic Properties of Nanoparticles.[27] This test evaluates the effect that CSA-SNPs have on the integrity of red blood cells by in vitro exposure and the quantification of hemoglobin released. First, hemoglobin standards were made covering a range of concentrations of 0.025−0.8 mg/L, and a standard curve was generated. Hemoglobin was oxidized to methemoglobin by ferricyanide in the presence of alkali. This concentration can be determined by measuring absorbance at 540 nm. Blood was diluted in PBS ($-Ca^{2+}/Mg^{2+}$) to a hemoglobin concentration of 10 mg/mL. In a test tube, 700 μL of PBS, 100 μL of diluted blood solution, and 100 μL of CSA-SNP solution were mixed and placed on an orbital shaker for 30 min. The samples were then placed in a water bath set to 37 °C for 3 h and 15 min. Next, samples were centrifuged for 15 min at 800*g*, and the supernatant was collected. Then, 100 μL of supernatant was added to a 96 well plate along with 100 μL of cyanmethemoglobin reagent. The mixture was covered, gently shaken, and allowed to react for 10 min; then, its absorbance at 540 nm was measured on a plate reader. This absorbance was compared to the standard curve to determine hemoglobin concentration. This concentration divided by the total hemoglobin concentration of the diluted blood solution yields percent hemolysis. A 10% Triton X solution was used as the positive control to determine total blood hemoglobin. Each sample was run in triplicate, and known standards were run with each sample to ensure they correlated properly with the standard curve.

2.2.7. Brightfield Imaging of Cell Morphology. To qualitatively assess cell health after CSA-SNP exposure, we seeded 3T3 fibroblasts with DMEM/10% FBS into 9 wells of a 12 well tissue culture treated plate and incubated them at 37 °C and 5% CO_2 until 50% confluent, about 2 days. The media were removed from all wells. Three of these wells were exposed to 600 μL of DMEM/10% FBS, three received 600 μL of a solution of CSA-SNPs in DMEM/10% FBS at 15 ppm, and three wells received 600 μL of a solution of CSA-SNPs in DMEM/10% FBS at 37 ppm. Samples were incubated for 24 h, again at 37 °C and 5% CO_2. Wells were imaged using a Nikon Eclipse TS100 Brightfield microscope (Melville, NY), Photometrics CoolSNAP camera (Tucson, AZ), and MetaMorph Advanced image analysis software.

2.2.8. Minimum Inhibitory Concentration and Minimum Bactericidal Concentration. The minimum inhibitory concentration (MIC) was determined using a protocol modified from that of Andrews.[28] Briefly, the inoculum was prepared by mixing one loop of the desired bacteria in 10 mL of MHB, which was then incubated at 37 °C overnight. The concentration of this inoculum was found to be 1.6×10^8 cfu/mL by plating serial dilutions. For testing, inoculum was used promptly that day and diluted to 1×10^6 cfu/mL. In preparation of the serially diluted 96 well plate, we added 100 μL of pure MHB to each well. Next, 100 μL of the antimicrobial solution, CSA-SNPs mixed in phosphate buffered saline (PBS) to 480 ppm, was added to the first well of each row. Then, using a multichannel pipet set to 100 μL, we serially diluted the CSA-SNP/MHB solution across the cell plate, thus making each consecutive well 50% the concentration of the preceding well. At this time, 100 μL of the prepared inoculum was added to each well, and the plate was incubated overnight. The MIC is defined as the most dilute concentration of an antimicrobial that will inhibit visible growth of a microbe after overnight incubation.[28,29] Each row should contain a live control/negative control (i.e., a well that contains no antimicrobial). Each row should also include a well consisting of only the pure MHB. This well should remain clear after incubation, thus ensuring that the MHB was not contaminated at any point in the study. These two controls also serve as a means of comparison for the treatment wells, one representing uninhibited growth and the other representing no growth. Minimum bactericidal concentration (MBC) was then determined using methods established by de Nooijer and Wallert and Provost Lab.[30,31] To each well of the 96 well plate with a concentration equal to or greater than that of the MIC, 40 μL of 5 ppm 3-(4,5-dimethyl-2-thiazolyl)-2,5-diphenyl-2*H*-tetrazolium bromide (MTT) was added, and the plate was incubated for 4 h at 37 °C. Any indication of color change from yellow to purple precipitate indicates viable bacteria. This can be confirmed by adding 150 μL of MTT solvent to each well and measuring absorbance at 590 nm; deviation in absorbance from a no-bacteria control will indicate viable bacteria are present. The most dilute concentration of antimicrobial agent that results in no viable bacteria is the MBC.[32] All trials were run in triplicate.

2.2.9. Time-Kill Assay. The rate of antimicrobial activity of CSA-SNP against *S. aureus* and *Escherichia coli* was examined using a time-kill assay modified from Isenberg.[33] The inoculum was prepared by mixing one loop of the desired bacteria in 10 mL of MHB, which was then incubated at 37 °C overnight. The concentration of this inoculum was found to be 1.6×10^8 cfu/mL by plating serial dilutions. For testing, inoculum was diluted to 1×10^6 cfu/mL and used promptly that day. Next, 100 μL of inoculated broth was added to each well on a 96 well plate. CSA-SNP suspended in DI water was added so that the final concentration in each well was 5, 10, 20, or 30 ppm. Immediately after exposure, 10 μL of alamarBlue (Invitrogen), as recommended by the producer, was added to one sample from each concentration; alamarBlue was sequentially added to the other wells at 1 h intervals thereafter. A negative control, representing uninhibited growth, was also included with each time group; this control consisted of only bacteria in MHB at the diluted concentration. The absorbance of each sample was read 3 h after exposure to alamarBlue using a Wallac 1420 VICTOR^2 Multilabel Counter (PerkinElmer). A 531 ± 25 nm filter was used for excitation, and a 593 ± 60 nm filter was used for emission. All trials were done in triplicate.

2.2.10. Confocal Imaging. Spatial selectivity of the CSA-SNPs to *S. aureus* was visualized using a Leica Microsystems DM IRE 2 confocal microscope system and corresponding software. *E. coli* and *S. aureus* were cultured in Mueller Hinton nutrient broth for 24 h at 37 °C. After incubation, *E. coli* and *S. aureus* were diluted to 1×10^7 cfu/mL; dilutions were made in sterile Mueller Hinton bacterial broth. Five hundred microliters of each dilution was then placed into the same well of a Lab-Tek II Chambered #1.5 German Coverglass System. The coculture of bacteria was allowed to affix to the slide for 1 h undisturbed. The solution was then removed. Next, the coculture was exposed to CSA-SNP diluted into PBS+ Ca^{2+} and Mg^{2+} at 24 mg/L. The coculture was exposed to the CSA-SNP on a wobble plate. This solution was removed after 30 min. The well was rinsed with 500 μL of PBS+ to remove excess nanoparticles. After the rinse was removed, the coculture was stained with Life Technologie LIVE BacLight Bacterial Gram Stain Kit. In accordance with the manufacturer's protocol, the stain was prepared by mixing 1.5 μL of BacLight component A (SYTO 9) and 1.5 μL of component B (hexidium iodide) into 500 μL of PBS− Ca^{2+} and Mg^{2+}. The bacteria were allowed to stain for 15 min in the dark and then imaged using Leica Microsystems DM IRE 2 confocal microscope system and software.

2.2.11. Image Analysis. Quantitative analysis was performed on the confocal and TEM images using the Image Processing Toolbox in MATLAB (MathWorks, Natick, MA). For TEM analysis, grayscale images were converted to binary images with a threshold calculated by Otsu's method. After we compared these images with the original images, we manually adjusted thresholds if necessary. Binary morphological operations were performed to identify nanoparticles, which were then counted as groups of connected pixels. Finally, effective diameters were estimated given a known area of pixels for each nanoparticle and assuming a circular cross section; n = 397 nanoparticles.

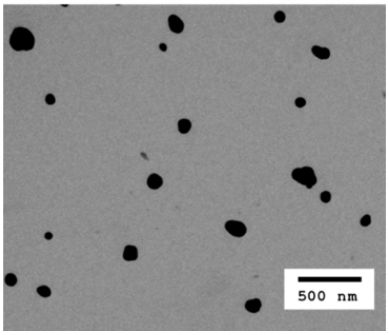

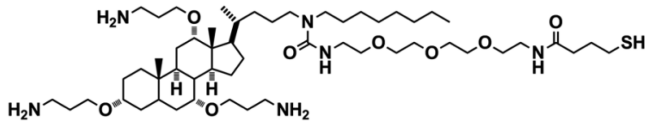

Figure 1. (Left) TEM of CSA-SNP and (right) CSA-124 structure.

For quantitative confocal analysis, images from each imaging channel were read into MATLAB. A threshold was again calculated by Otsu's method and modified manually after comparison with the overlay of the three channels (due to differential uptake of each stain, cell morphology was used when necessary to aid in manual threshold determination). Next, the centroids of isolated objects (*S. aureus* cells, *E. coli*, and silver nanoparticles) in each channel were identified. Using the two-dimensional distance formula, the distance from the centroid of a single nanoparticle to the centroid of every *S. aureus* and *E. coli* bacterium was calculated; the minimum distance of those calculated for *S. aureus* and *E. coli* represents the closest *S. aureus* and *E. coli* bacterium, respectively, to that nanoparticle. This process was repeated for each nanoparticle in the image. Statistical analysis, specifically Student's *t* test for significance and Ripley's *K*-function for clustering, were performed.

2.2.12. Optical Trapping. The instrument (MMI CellManipulator, MMI, Zurich, Switzerland) was fabricated to work as an optical trapping system with force measurement capabilities. The optical trapping laser used was an 8 W Nd:YAG (yttrium−aluminum−garnet) laser emitting light at a wavelength of 1070 nm. The laser beam used was expanded to maximally illuminate the back aperture of the microscope objective. The objective used was a 100× plan fluor objective (Nikon Instruments). A galvanometer that could create multiple individual traps simultaneously using a time-sharing mode was used. The instrument was designed as an optical trapping system using a Nikon TE2000 for imaging. Also, for this study, CSA functionalized microparticles (CSA-MP) were synthesized from polystyrene beads functionalized with a colloidal silver shell and CSA-124. These particles share the same surface chemistry as the CSA-SNP but are larger, typically 1 μm. This larger size facilitates optical capture and imaging

A glass slide was passivated with dried milk, and a diluted sample of CSA-MP and *S. aureus* was placed on the surface. The slide was then sealed with a glass coverslip and parafilm. The slide was then placed under a 100× oil immersion objective, and the laser was turned on. Two traps were created, one for a single bacterium and another for a CSA-MP nanoparticle. The laser power was adjusted to about 30% to minimize potential spurious laser interactions and heating. The trap containing the bacterium was slowly moved to approach the *S. aureus* to eventual contact, as indicated by slight displacement of both. In this series of measurements, the staph/CSA-NP adduct was annealed about 2 s before moving the traps apart. The same procedure was followed with identical beads that did not contain CSA-124. Results reported are based on an average of 200 trials repeated over 80 sets of independently prepared microscope slides.

3. RESULTS AND DISCUSSION

Nanoparticle size was determined through TEM image analysis and DLS (Figure 1). These results are reported in Table 1. As expected, the hydrodynamic diameter determined via DLS is greater than the diameter determined via TEM due to the presence of solvated surfactant on the particle surface because the former is a weight-average technique. Also of note is that

Table 1. Nanoparticle Characterization

parameter	HPC-SNP	CSA-SNP
SNP diameter via TEM analysis (nm)	68 ± 18	64 ± 38
hydrodynamic diameter (nm)	81.9 ± 9.4	102.2 ± 2.3
zeta potential (mV)	−18.23 ± 0.83	−8.34 ± 1.05

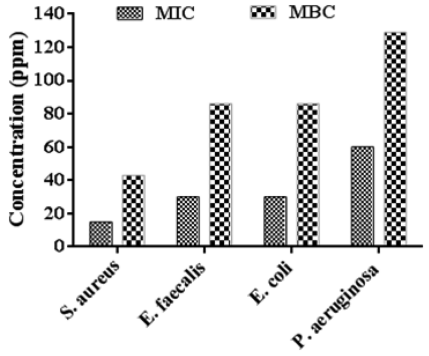

Figure 2. MIC and MBC of CSA-SNP against various bacteria.

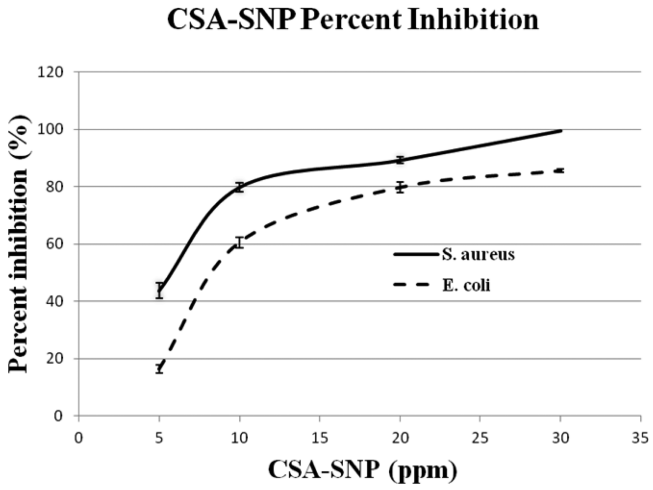

Figure 3. Time-kill assay showing increased inhibition of *S. aureus* versus *E. coli* due to CSA-SNPs. Percent inhibition is with respect to unexposed live controls.

the hydrodynamic diameter increased as the positively charged CSA-124 molecules were added to the system, indicating self-assembly on the nanoparticle surface. While precise size and distribution of CSA-SNPs are not critical in these experiments, they are relevant to colloidal stability and in vivo biocompatibility. Larger particles are more likely to settle from solution, potentially irreversibly aggregating and increasing apparent size.

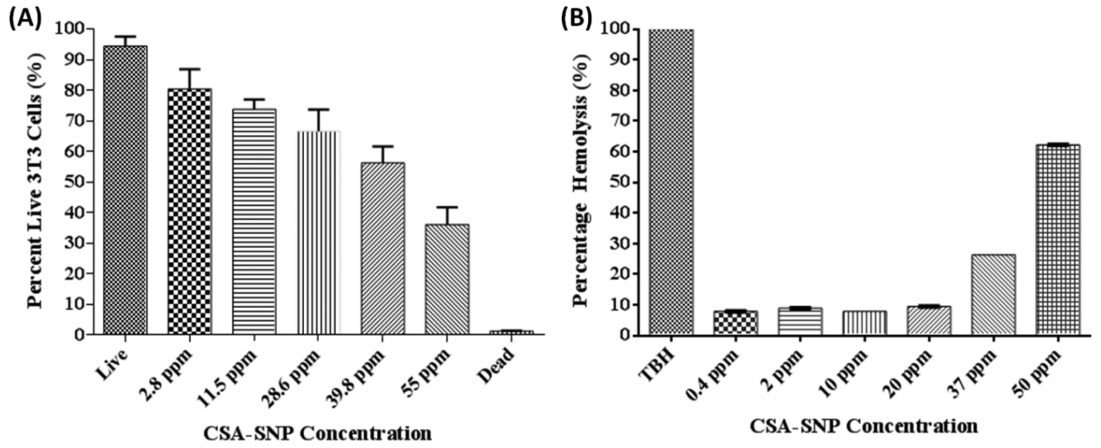

Figure 4. (A) Cytotoxicity of CSA-SNPs. (B) Hemolytic activity of CSA-SNPs.

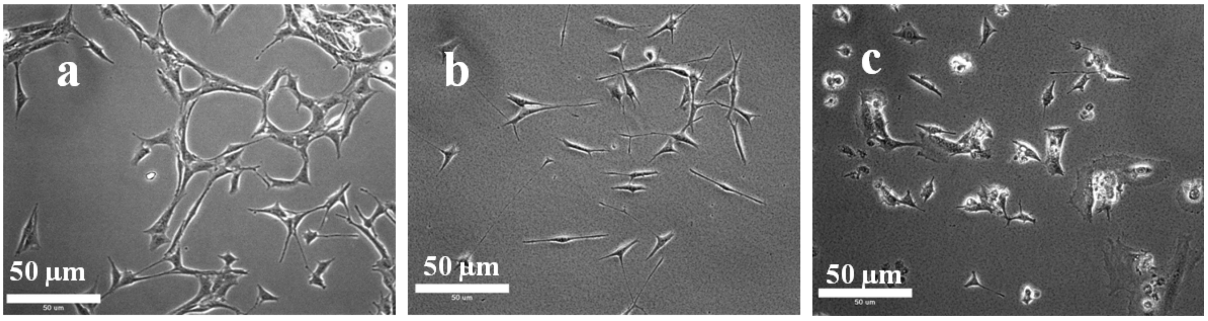

Figure 5. Bright-field images of 3T3 fibroblasts that received (a) 0 ppm of CSA-SNP, (b) 15 ppm of CSA-SNP, and (c) 37 ppm of CSA-SNP.

Also, nanoparticles possessing a diameter greater than 200 nm are more prone to activate the complement system and thus be cleared from the circulatory system.[34] Nanoparticles with a diameter under 100 nm are capable of penetrating blood vessel pores, and NPs under 20 nm can access interstitial spaces.[11] This characteristic has been termed the enhanced permeability and retention (EPR) effect.[35,36]

As expected, the nanoparticle gains positive charge after the addition of CSA, due to the three ammonium groups on CSA-124 in neutral media. This data supports the fact that CSA was successfully conjugated to the nanoparticle surface. It is also relevant because the nature of the surface charge also affects the nanoparticles' in vitro and in vivo interactions. Particles with a moderately neutral charge will be more likely to agglomerate, resulting in shorter shelf lives, a lower solubility threshold, and an increased probability of removal from in vivo circulation.[37] Once in the body, nanoparticles are susceptible to opsonization, recognition, and removal by the mononuclear phagocyte system (MPS). In general, neutral to negatively charged nanoparticles with hydrophilic polymer surfaces exhibit prolonged circulation times.[34]

An appealing quality of the CSA-SNP is the ease of noble metal nanoparticle conjugation. CSA-124 has been specifically synthesized with a thiol-terminated polyethylene glycol side chain that favorably binds to noble metals. The SmartSilverAS silver nanoparticles, from this point referred to as SNPs, used for this procedure are stabilized with hydroxypropyl cellulose (HPC), which provides the nanoparticles with high solubility in aqueous and organic alcohol solvent systems and increases biocompatibility. Because CSA-124 has greater thermodynamic and steric stability than HPC on the surface of the SNPs, CSA-124 spontaneously displaces a portion of the HPC molecules.

For the quantification of CSA-124 bound to the SNP surface, we first constructed a standard curve of integrated peak area versus known CSA concentration using HPLC−ESI-TOF-MS (Supporting Information). The CSA was displaced from the SNP surface using DTT; the particles were separated by centrifugation and analyzed using HPLC−ESI-TOF-MS. The corresponding CSA concentration was determined to be 1.5 mg/L for a 500 μL sample, or 4.52×10^{14} CSA molecules. Using ICP-OES and estimates of particle size from TEM, we determined the same 500 μL sample contained 1.32×10^{11} SNPs, and thus, we conclude there are on average 3424 CSA-124 molecules bound to each SNP.[38] Future work will concentrate on optimizing this parameter.

The antimicrobial results for the minimum inhibitory concentration (MIC) and minimum bactericidal concentration (MBC) are reported in Figure 2. As the graph indicates, CSA-SNPs demonstrate similar efficacy against *S. aureus* (MIC 15 ppm), *E. faecalis* and *E. coli* (MIC 30 ppm), and *P. aeruginosa* (MIC 60 ppm). Our own determination of the MIC of SNPs was obtained using the same protocol as above and found to be roughly 250 ppm for both *S. aureus* and *E. coli*. While this study demonstrates that a CSA-SNP conjugate is a more potent antimicrobial than an SNP alone, it does not attempt to elucidate the mechanistic roles of each component, as potential mechanisms of each have previously been published. Antimicrobial properties of CSA have been attributed to membrane disruption through depolarization and permeabilization, while SNPs have been demonstrated to disrupt cell wall synthesis, membrane ion pumps, translation, and nucleic acid synthesis.[5,14−17,25,39] Also of note, Kim et al. reported that SNPs alone inhibited *E. coli* 10 times more effectively than *S. aureus*, suggesting the CSA may impart SNPs with some

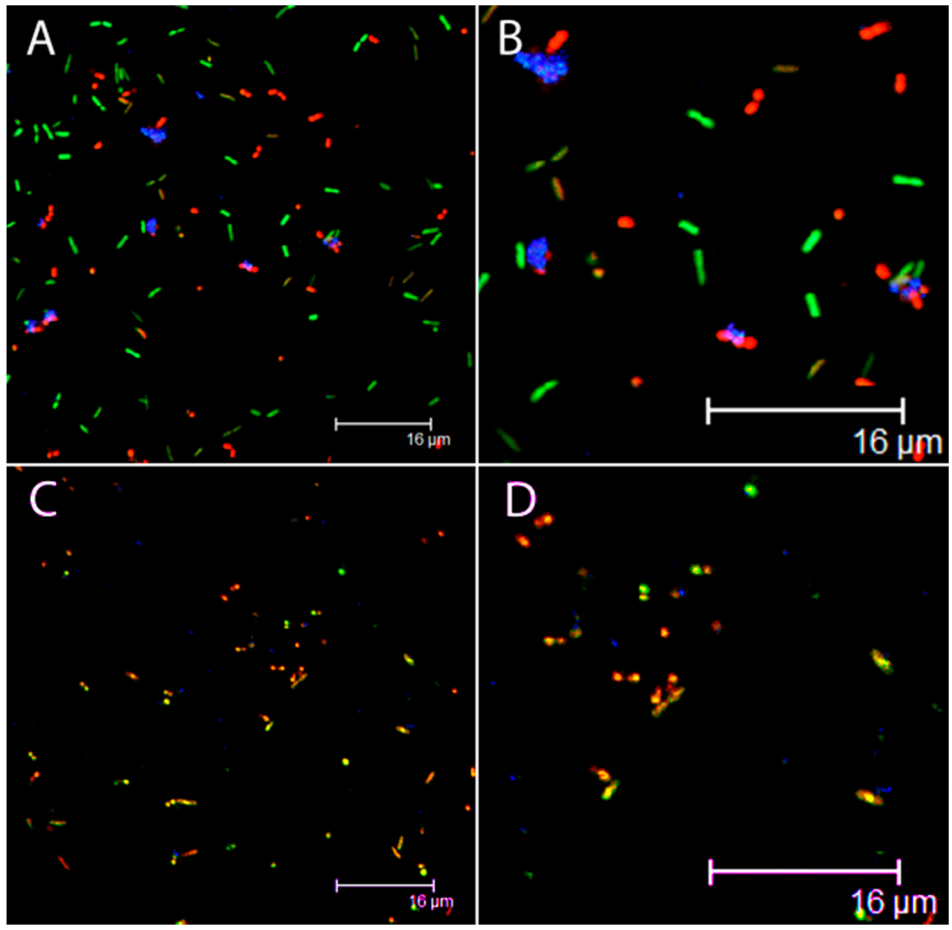

Figure 6. Confocal imaging of (red) *S. aureus*, (green) *E. coli*, and (blue) nanoparticles. (A and B) CSA-SNPs and (C and D) unmodified SNPs. (B and D) Enlarged segments of A and C, respectively.

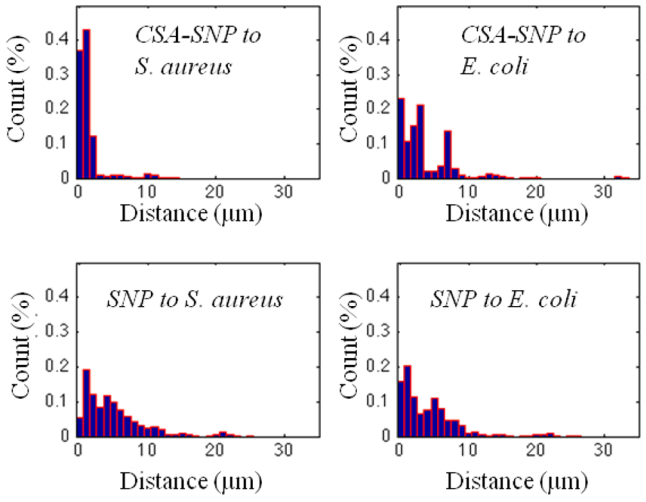

Figure 7. Histograms of (top) experimental and (bottom) negative control distances from SNPs to (left) *S. aureus* and (right) *E. coli*.

Table 2. Statistics from Quantitative Image Analyses

samples	av distance from NP to cell (μm)
CSA-SNP to *S. aureus*	1.283 ± 1.994
CSA-SNP to *E. coli*	3.489 ± 3.883
SNP (neg. control) to *S. aureus*	4.864 ± 4.393
SNP (neg. control) to *E. coli*	3.991 ± 4.165

mechanism of selectivity.[14] Further evidence of physical selectivity was given by confocal imaging of cocultures of these bacteria. Statistical analysis using MATLAB demonstrated that CSA-SNPs were more likely to be near *S. aureus* than *E. coli*. This could be due in part to electrostatic attraction between the cationic CSA and the negatively charged peptidoglycan, which Gram-positive bacteria express in much greater quantities.[40] It has been well demonstrated that different cell types present different membrane constituents to its surrounding environment, which influences how the cell responds to extracellular foreign bodies, a concept known as cell vision. This phenomenon impacts the surface binding, cellular uptake, and internal fate of nanoparticles and in part explains the drastic differences in NP response among various cell types.[41,42] Further antimicrobial characterization was provided through a time-kill study, depicted in Figure 3.

As depicted in Figure 3, minimal inhibition is seen at 5 ppm, and efficacy increases as concentration increases. Note that inhibition results of the time-kill assay vary slightly from those of the MIC, as this was a 4 h study and MIC is a 24 h study. The results of the time-kill assay echo those of the MIC/MBC in that *S. aureus* shows increased sensitivity to CSA-SNPs compared to *E. coli*.

The concentration dependent toxicity of CSA-SNPs to mouse 3T3 fibroblasts was determined by cell treatment followed by flow cytometry and is presented in Figure 4. The CSA-SNPs show very limited toxicity below 39.8 ppm and reach the 50% viability threshold at ~50 ppm. The differences

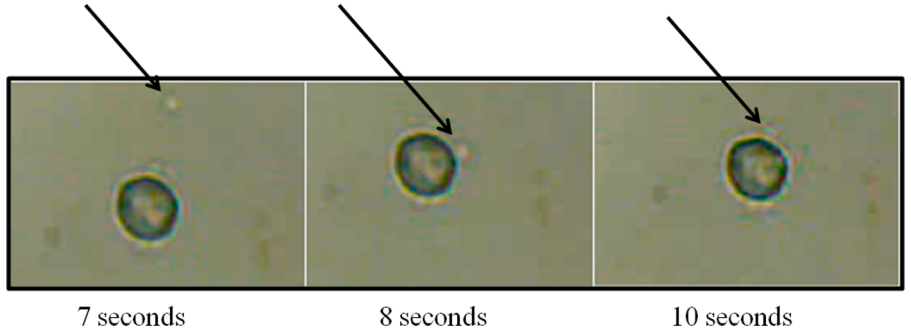

Figure 8. *S. aureus* (indicated with arrows) adhering to CSA functionalized MP.

between the live control and the 39.8 and 55 ppm samples were found to be significant by one-way ANOVA with Bonferroni's posttest ($p < 0.05$). The hemolytic assay shows nearly identical results with increasing hemolysis at 37.5 ppm and slightly over 50% hemolysis occurring at 50 ppm. The differences between the TBH, 37 ppm, and 50 ppm samples were found to be significant from all other samples as determined by one-way ANOVA with Bonferroni's posttest ($p < 0.05$). These findings suggest about a 3-fold difference between MIC and EC_{50tox} for *S. aureus* and 3T3 cells, respectively. Simultaneous testing of SNPs alone showed little cytotoxicity up to 200 ppm. This result is supported by the work of Jain et al., who reported that the IC_{50} for SNPs against Hep G2 cells to be 251 ppm. These findings suggest that CSA-SNPs are roughly 5 times more toxic to 3T3 cells than SNPs alone.[43]

The cytotoxic effects of CSA-SNPs were also qualitatively assessed via bright-field imaging. In Figure 5a, the typical spindle morphology of healthy 3T3 fibroblast cells can be seen. In Figure 5b, representing the MIC of *S. aureus* at 15 ppm of CSA-SNP, the cells appear to have slightly reduced size but retain their characteristic spindle morphology. CSA-SNP at 37 ppm results in stark contrast in cell morphology indicative of cytotoxicity. These results are consistent with those from the hemolysis and flow cytometry studies.

Qualitative image analysis of the confocal overlays (Figure 6) suggests that the CSA-SNPs are distributed spatially closer to *S. aureus* cells than to *E. coli* cells. Analysis of these images provides the closest *S. aureus* and *E. coli* to each SNP; histograms and simple statistics are shown in Figure 7 and Table 2, respectively.

Table 2 illustrates the distribution of distances for both experimental and negative control groups. The difference in average distance between CSA-SNP and *S. aureus* versus CSA-SNP and *E. coli* is statistically significant, as is the difference in average distance between the CSA-SNP treatment samples and the SNP negative control samples (two-way *t* test, $p < 0.05$). More than 70% of the CSA-SNPs are within 2 μm of an *S. aureus* cell, whereas less than 40% of CSA-SNPs are within 2 μm of an *E. coli* cell. CSA-SNPs also show a higher incidence at distances greater than 5 μm from *E. coli* than from *S. aureus*. This is confirmed by the averages and standard deviations shown in Table 2; CSA-SNPs, on average, are closer to *S. aureus* than to *E. coli*. The standard deviations indicate less dispersion among the CSA-SNP to *S. aureus* data than the CSA-SNP to *E. coli* data. Ripley's *K*-function clustering analysis indicates that the CSA-SNPs are spatially clustered, particularly on shorter scales.

The negative control data show no significant difference between the SNP to *S. aureus* distance and the SNP to *E. coli* distance. This is highlighted by large standard deviations for both negative control groups. However, statistically, the mean CSA-SNP to *S. aureus* distance is significantly different from the SNP to *S. aureus* average distance.

Selectivity was then qualitatively demonstrated on the scale of single cells through video observation and optical trapping technology. Optical trapping has the capability to manipulate small living biological objects, such as single bacterial cells, as well as inanimate particles. The infrared wavelength is minimally invasive to living cells. The optical trapping at a cellular level provides insight into biological interactions. Therefore, optical trapping of CSA-SNP and *S. aureus* was performed to further investigate the interactions and potential selectivity.

Video clip 1 (Supporting Information) is an 18 frame movie. The compressed video clip can be replayed frame by frame in Windows Media Player. Initially, *S. aureus* is trapped in the upper left corner, and a CSA-MP is trapped in the middle of the screen. In frames 3−6, the *S. aureus* is manipulated to slowly approach the CSA-MP and allowed to incubate for <1 s. The trap is then moved, but the bacterium remains adhered to CSA-124. In frames 7−10 and 10−13, the procedure is repeated, and two more bacteria adhere to the same CSA-MP.

An optical trap was used to show the adhesion of CSA-MP to *S. aureus* (Figure 8). A single bacterium was trapped in one specific trap, and CSA-MP was simultaneously trapped in another trap. The bacteria were manually moved to approach the CSA-MP. The bacteria were then allowed to touch and reside for several seconds, and then the two traps were moved apart. The result was the *S. aureus* remained attached and was not able to be displaced by the force of the optical trap. The video shows that three separate bacteria can attach and bind to one CSA functionalized particle. Repeated trials indicated that interactions generally formed within periods of <2 s. As a control, the procedure was repeated with nanoparticles lacking CSA-124 surfactant. The nanoparticles without CSA-124 did not manifest adhesion to *S. aureus*, even when extending the residence time beyond 10 s.

4. CONCLUSION

Silver has been used clinically as a broad-spectrum antimicrobial since it was approved by the FDA in the 1920s.[43] Recent research indicates that there are many downsides to broad-spectrum antimicrobials including longer recovery times, increased risk of further infection, and higher incidence of drug resistance. The data presented suggest that the antimicrobial qualities of silver can be complemented via conjugation with selective ligands such as CSA-124. While SNPs alone have an MIC of 120 ppm against *S. aureus*, CSA-

SNPs express an MIC of 15 and 30 ppm toward *S. aureus* and *E. faecalis*, respectively, and an MIC of 30 and 60 ppm toward *E. coli* and *P. aeruginosa*, respectively. This work further suggests that the functionalization of CSA to the nanoparticle surface imparts spatial selectivity in favor of *S. aureus* over *E. coli*; however, spatial selectivity does not necessarily imply antimicrobial selectivity. These findings were further supported through MATLAB analysis of confocal images, indicating that while in coculture, 70% of CSA-SNPs were within 2 μm of an *S. aureus* cell while less than 40% were within 2 μm of an *E. coli* cell. Video images of laser captured nanoparticle interactions with both bacteria also show clear selectivity for the Gram-positive *S. aureus* over the Gram-negative *E. coli*. Future work will focus on optimizing ligand concentration, verifying the mechanism of ligand affinity, and improving compatibility.

■ ASSOCIATED CONTENT

Supporting Information

Videos of CSA-MP interactions with *S. aureus* and *E. coli*. This material is available free of charge via the Internet at http://pubs.acs.org.

■ AUTHOR INFORMATION

Corresponding Author

*E-mail: danielhayes@lsu.edu. Tel.: (225) 578-3153. Fax: (225) 578-2919.

Present Address

⊥Ammar Qureshi: Henry M. Jackson Foundation for the Advancement of Military Medicine, Silver Spring, MD 20910

Thomas Scherr: Vanderbilt University, Department of Biomedical Engineering, 2301 Vanderbilt Place, Nashville, TN 37235-1826.

Author Contributions

The manuscript was written through the contributions of all authors. All authors have given approval to the final version of this manuscript.

Notes

The authors declare no competing financial interest.

■ ACKNOWLEDGMENTS

The authors would like to acknowledge the following personnel for services rendered: Ms. Connie David for HPLC−ESI-TOF-MS diagnostics; Dr. Yubo Li for CSA-124 synthesis; Timothy Machen for aid in the hemolysis study; and Katie Hogan for assisting in 3T3 cell culture, cytotoxicity study, and the time-kill assay. Financial support for this study was provided by the National Science Foundation (Proposals CMMI-963482 and CBET-1254281) and from the LSU AgCenter.

■ REFERENCES

(1) Guarner, F.; Malagelada, J.-R. Gut Flora in Health and Disease. *Lancet* **2003**, *361* (9356), 512−519.

(2) Kelly, C. P.; Pothoulakis, C.; LaMont, J. T. *Clostridium difficile* Colitis. *N. Engl. J. Med.* **1994**, *330* (4), 257−262.

(3) Bignardi, G. Risk Factors for *Clostridium difficile* Infection. *J. Hosp. Infect.* **1998**, *40* (1), 1.

(4) Eckert, R.; He, J.; Yarbrough, D. K.; Qi, F.; Anderson, M. H.; Shi, W. Targeted Killing of *Streptococcus mutans* by a Pheromone-Guided "Smart" Antimicrobial Peptide. *Antimicrob. Agents Chemother.* **2006**, *50* (11), 3651−3657.

(5) Travan, A.; Pelillo, C.; Donati, I.; Marsich, E.; Benincasa, M.; Scarpa, T.; Semeraro, S.; Turco, G.; Gennaro, R.; Paoletti, S. Non-cytotoxic Silver Nanoparticle−Polysaccharide Nanocomposites with Antimicrobial Activity. *Biomacromolecules* **2009**, *10* (6), 1429−1435.

(6) Pal, S.; Tak, Y. K.; Song, J. M. Does the Antibacterial Activity of Silver Nanoparticles Depend on the Shape of the Nanoparticle? A Study of the Gram-Negative Bacterium *Escherichia coli*. *Appl. Environ. Microbiol.* **2007**, *73* (6), 1712−1720.

(7) Yih, T.; Al-Fandi, M. Engineered Nanoparticles as Precise Drug Delivery Systems. *J. Cell. Biochem.* **2006**, *97* (6), 1184−1190.

(8) Minchin, R. F.; Martin, D. J. Minireview: Nanoparticles for Molecular Imaging—An Overview. *Endocrinology* **2010**, *151* (2), 474−481.

(9) Singh, R.; Lillard, J. W., Jr. Nanoparticle-Based Targeted Drug Delivery. *Exp. Mol. Pathol.* **2009**, *86* (3), 215−223.

(10) Gelperina, S.; Kisich, K.; Iseman, M. D.; Heifets, L. The Potential Advantages of Nanoparticle Drug Delivery Systems in Chemotherapy of Tuberculosis. *Am. J. Respir. Crit. Care Med.* **2005**, *172* (12), 1487−1490.

(11) Emerich, D. F.; Thanos, C. G. The Pinpoint Promise of Nanoparticle-Based Drug Delivery and Molecular Diagnosis. *Biomol. Eng.* **2006**, *23* (4), 171−184.

(12) Love, J. C.; Estroff, L. A.; Kriebel, J. K.; Nuzzo, R. G.; Whitesides, G. M. Self-Assembled Monolayers of Thiolates on Metals as a Form of Nanotechnology. *Chem. Rev.* **2005**, *105* (4), 1103−1170.

(13) Brown, P. K.; Qureshi, A. T.; Moll, A. N.; Hayes, D. J.; Monroe, W. T. Silver Nanoscale Antisense Drug Delivery System for Photoactivated Gene Silencing. *ACS Nano* **2013**, *7* (4), 2948−2959.

(14) Kim, J. S.; Kuk, E.; Yu, K. N.; Kim, J.-H.; Park, S. J.; Lee, H. J.; Kim, S. H.; Park, Y. K.; Park, Y. H.; Hwang, C.-Y. Antimicrobial Effects of Silver Nanoparticles. *J. Nanomed. Nanotechnol.* **2007**, *3* (1), 95−101.

(15) Lok, C.-N.; Ho, C.-M.; Chen, R.; He, Q.-Y.; Yu, W.-Y.; Sun, H.; Tam, P. K.-H.; Chiu, J.-F.; Che, C.-M. Silver Nanoparticles: Partial Oxidation and Antibacterial Activities. *J. Biol. Inorg. Chem.* **2007**, *12* (4), 527−534.

(16) Baker, T. B.; McFall, R. M.; Shoham, V. Current Status and Future Prospects of Clinical Psychology Toward a Scientifically Principled Approach to Mental and Behavioral Health Care. *Psychol. Sci. Public Interest* **2009**, *9* (2), 67−103.

(17) Aymonier, C.; Schlotterbeck, U.; Antonietti, L.; Zacharias, P.; Thomann, R.; Tiller, J. C.; Mecking, S. Hybrids of Silver Nanoparticles with Amphiphilic Hyperbranched Macromolecules Exhibiting Antimicrobial Properties. *Chem. Commun.* **2002**, *24*, 3018−3019.

(18) Gibbins, B.; Warner, L. The Role of Antimicrobial Silver Nanotechnology. *Med. Device Diagn. Ind.* **2005**, *1*, 1−2.

(19) Silver, S.; Phung, L. T.; Silver, G. Silver as Biocides in Burn and Wound Dressings and Bacterial Resistance to Silver Compounds. *J. Ind. Microbiol. Biotechnol.* **2006**, *33* (7), 627−634.

(20) Hancock, R.; Patrzykat, A. Clinical Development of Cationic Antimicrobial Peptides: From Natural to Novel Antibiotics. *Curr. Drug Targets: Infect. Disord.* **2002**, *2* (1), 79−83.

(21) Zasloff, M. Antimicrobial Peptides of Multicellular Organisms. *Nature* **2002**, *415* (6870), 389−395.

(22) Epand, R. M.; Epand, R. F.; Savage, P. B. Ceragenins (Cationic Steroid Compounds), A Novel Class of Antimicrobial Agents. *Drug News Perspect.* **2008**, *21* (6), 307−11.

(23) Chin, J. N.; Jones, R. N.; Sader, H. S.; Savage, P. B.; Rybak, M. J. Potential Synergy Activity of the Novel Ceragenin, CSA-13, Against Clinical Isolates of *Pseudomonas aeruginosa*, Including Multidrug-Resistant *P. aeruginosa*. *J. Antimicrob. Chemother.* **2008**, *61* (2), 365−370.

(24) Leszczyńska, K.; Namiot, A.; Fein, D. E.; Wen, Q.; Namiot, Z.; Savage, P. B.; Diamond, S.; Janmey, P. A.; Bucki, R. Bactericidal Activities of the Cationic Steroid CSA-13 and the Cathelicidin Peptide LL-37 Against *Helicobacter pylori* in Simulated Gastric Juice. *BMC Microbiol.* **2009**, *9* (1), 187.

(25) Chin, J. N.; Rybak, M. J.; Cheung, C. M.; Savage, P. B. Antimicrobial Activities of Ceragenins Against Clinical Isolates of Resistant Staphylococcus aureus. *Antimicrob. Agents Chemother.* **2007**, *51* (4), 1268−1273.

(26) Leszczyńska, K.; Namiot, D.; Byfield, F. J.; Cruz, K.; Żendzian-Piotrowska, M.; Fein, D. E.; Savage, P. B.; Diamond, S.; McCulloch, C. A.; Janmey, P. A. Antibacterial Activity of the Human Host Defence Peptide LL-37 and Selected Synthetic Cationic Lipids Against Bacteria Associated with Oral and Upper Respiratory Tract Infections. *Antimicrob. Agents Chemother.* **2013**, *68* (3), 610−618.
(27) Standard Test Method for Analysis of Hemolytic Properties of Nanoparticles. In *International Committee for Standardization in Haemotology*; ASTM International: West Conshohocken, PA, 1979; Vol. *E2524−08*.
(28) Andrews, J. M. Determination of Minimum Inhibitory Concentrations. *Antimicrob. Agents Chemother.* **2001**, *48* (Suppl. 1), 5−16.
(29) Wiegand, I.; Hilpert, K.; Hancock, R. E. Agar and Broth Dilution Methods to Determine the Minimal Inhibitory Concentration (MIC) of Antimicrobial Substances. *Nat. Protoc.* **2008**, *3* (2), 163−175.
(30) Seligy, V.; Rancourt, J. Antibiotic MIC/MBC Analysis of Bacillus-Based Commercial Insecticides: Use of Bioreduction and DNA-Based Assays. *J. Ind. Microbiol. Biotechnol.* **1999**, *22* (6), 565−574.
(31) de Nooijer, L. J.; Duijnstee, I.; Van der Zwaan, G. Novel Application of MTT Reduction: A Viability Assay for Temperate Shallow-Water Benthic Foraminifera. *J. Foraminiferal Res.* **2006**, *36* (3), 195−200.
(32) Taylor, P.; Schoenknecht, F.; Sherris, J.; Linner, E. Determination of Minimum Bactericidal Concentrations of Oxacillin for *Staphylococcus aureus*: Influence and Significance of Technical Factors. *Antimicrob. Agents Chemother.* **1983**, *23* (1), 142−150.
(33) Isenberg, H. D., Ed. *Clinical Microbiology Procedures Handbook*; ASM Press: Washington, DC, 2007.
(34) Perry, J.; Reuter, K. G.; Kai, M. P.; Herlihy, K. P.; Jones, S. W.; Luft, J. C.; Napier, M. E.; Bear, J. E.; DeSimone, J. M. PEGylated PRINT Nanoparticles: The Impact of PEG Density on Protein Binding, Macrophage Association, Biodistribution, and Pharmacokinetics. *Nano Lett.* **2012**, *12* (10), 5304−5310.
(35) Agasti, S. S.; Chompoosor, A.; You, C. C.; Ghosh, P.; Kim, C. K.; Rotello, V. M. Photoregulated Release of Caged Anticancer Drugs from Gold Nanoparticles. *J. Am. Chem. Soc.* **2009**, *131* (16), 5728−5729.
(36) Chertok, B.; Moffat, B. A.; David, A. E.; Yu, F.; Bergemann, C.; Ross, B. D.; Yang, V. C. Iron Oxide Nanoparticles as a Drug Delivery Vehicle for MRI Monitored Magnetic Targeting of Brain Tumors. *Biomaterials* **2008**, *29* (4), 487−496.
(37) Moghadam, B. Y.; Hou, W. C.; Corredor, C.; Westerhoff, P.; Posner, J. The Role of Nanoparticle Surface Functionality in the Disruption of Model Cell Membranes. *Langmuir* **2012**, *28* (47), 16318−16326.
(38) Brown, P. K.; Qureshi, A. T.; Moll, A. N.; Hayes, D. J.; Monroe, W. T. Silver Nanoscale Antisense Drug Delivery System for Photoactivated Gene Silencing. *ACS Nano* **2013**, *7* (4), 2948−2959.
(39) Ding, B.; Guan, Q.; Walsh, J. P.; Boswell, J. S.; Winter, T. W.; Winter, E. S.; Boyd, S. S.; Li, C.; Savage, P. B. Correlation of the Antibacterial Activities of Cationic Peptide Antibiotics and Cationic Steroid Antibiotics 1. *J. Med. Chem.* **2002**, *45* (3), 663−669.
(40) Morones, J. R.; Elechiguerra, J. L.; Camacho, A.; Holt, K.; Kouri, J. B.; Ramírez, J. T.; Yacaman, M. J. The Bactericidal Effect of Silver Nanoparticles. *Nanotechnology* **2005**, *16* (10), 2346.
(41) Mahmoudi, M.; Laurent, S.; Shokrgozar, M. A.; Hosseinkhani, M. Toxicity Evaluations of Superparamagnetic Iron Oxide Nanoparticles: Cell "Vision" Versus Physicochemical Properties of Nanoparticles. *ACS Nano* **2011**, *5* (9), 7263−7276.
(42) Laurent, S.; Burtea, C.; Thirifays, C.; Häfeli, U. O.; Mahmoudi, M. Crucial Ignored Parameters on Nanotoxicology: The Importance of Toxicity Assay Modifications and "Cell Vision. *PLoS One* **2012**, *7* (1), e29997.
(43) Jain, J.; Arora, S.; Rajwade, J. M.; Omray, P.; Khandelwal, S.; Paknikar, K. M. Silver Nanoparticles in Therapeutics: Development of an Antimicrobial Gel Formulation for Topical Use. *Mol. Pharmaceutics* **2009**, *6* (5), 1388−1401.